Electrochemistry Communications 135 (2022) 107221

Contents lists available at ScienceDirect

Electrochemistry Communications

journal homepage: www.elsevier.com/locate/elecom

Full Communication

Immobilization of FeFe-hydrogenase on black TiO_2 nanotubes as biocathodes for the hydrogen evolution reaction

Xin Liu [a], Sanne Risbakk [b], Patricia Almeida Carvalho [c], Mingyi Yang [b], Paul Hoff Backe [b], Magnar Bjørås [b], Truls Norby [a], Athanasios Chatzitakis [a,*]

[a] Centre for Materials Science and Nanotechnology, Department of Chemistry, University of Oslo, Gaustadalléen 21, NO-0349 Oslo, Norway
[b] Department of Microbiology, Oslo University Hospital HF, NO-0372 Oslo, Norway
[c] SINTEF Industry, POB 124 Blindern, NO-0314 Oslo, Norway

ARTICLE INFO

Keywords:
FeFe-hydrogenase
Bio-inorganic electrode
Enzyme immobilization
Direct electron transfer
TiO_2 nanotubes
Black TiO_2

ABSTRACT

Hydrogenases are attractive biocatalysts for utilization in electrochemical devices as potential replacement for Pt in hydrogen evolving electrodes. In this work, we investigate the immobilization of ferredoxin tagged FeFe-hydrogenase (Fd-HydA1) on black TiO_2 nanotubes (bTNTs), with uniform nanotube opening diameters of 140 nm. By utilizing an immunogold labelling method, we show that the enzymes attach on the top surface of the bTNTs film rather than on the inner nanotube walls, reflecting the difficulty to insert enzymes into high aspect-ratio nanomaterials for O_2-shielding. Nevertheless, cyclic voltammetry demonstrates direct electron transfer between Fd-HydA1 and bTNTs for the hydrogen evolution reaction (HER) in neutral media. This work provides new insight towards design of new nanostructured electrodes for enzyme immobilization.

1. Introduction

FeFe-hydrogenases are metallo-enzymes constituted by earth abundant elements that under anaerobic conditions catalyse the H_2 evolution from protons and electrons with an activity superior to that of Pt [1]. However, these biocatalysts rely heavily upon redox mediators to transfer electrons, such as viologens, which are expensive and toxic, greatly limiting their usage in electrolysis systems at large scale [2]. Enzyme immobilization on appropriate substrate materials can contribute to direct electron transfer (DET) between the enzyme and the solid support, alleviating the need for electron mediators. Additionally, the enzyme immobilization enables the reusability of the enzymes and could provide a shielding environment to enhance their stability [3,4].

High enzyme loading increases the probability of molecular orientation(s) suitable for efficient electron transfer to the solid support, as required to drive the electrochemical processes at high catalytic currents in practical implementations of bioelectrodes. Immobilization of hydrogenases has been studied over a wide range of carbon-based materials, such as pyrolytic graphite edge (PGE) and glassy carbon, enabling catalytic studies with the use of rotating disc electrodes, but enzyme loading has been typically low [5,6]. To increase loading, the support materials should provide high surface-to-volume ratio. Numerous porous polymers [7], silica [8] and metal-oxide based materials [9] have been implemented as support materials. Macroporous materials with pore diameters over 50 nm have been deemed most suitable, as they provide spatial unrestricted access for enzyme molecules entering the pores [4]. However, correlations between nano-material architectures and enzyme loadings have been far less explored and there is still no direct evidence that the enhanced enzyme immobilization in macroporous materials stems from the insertion of enzymes into the pores.

TiO_2 has been reported as the substrate material to immobilize hydrogenase in combination with a photoanode [10], and DET between bio-inorganic interfaces has been confirmed [11,12]. TiO_2 nanotubes (TNTs) exhibit high diversity in tube morphologies [13,14], while their high surface area and unique architecture provide the opportunity to further enhance enzyme loading and stability. In this work, we synthesized highly ordered nanostructured TiO_2 nanotubes (TNTs) as substrate material to investigate Fd-HydA1 immobilization. In order to implement TNTs as the substrate material, we utilized CaH_2 as reductant. The resulting TNTs have black appearance (bTNTs) and metallic-like behaviour, therefore being suitable as substrate materials for HydA immobilization and possible DET for the HER [15,16]. The bTNTs have a uniform tube opening diameter of 140 nm and a tube length of around 1 μm. The attachment of enzyme molecules on the internal walls of bTNTs

* Corresponding author.
E-mail address: athanasios.chatzitakis@smn.uio.no (A. Chatzitakis).

https://doi.org/10.1016/j.elecom.2022.107221

Available online 22 January 2022

is further studied by immunogold labelling electron microscopy. Vacuum infiltration and magnetic fields were employed to assist the loading process.

2. Experimental

2.1. Black TiO_2 nanotube synthesis

A two-step electrochemical anodization process was performed with titanium (Ti) foil (Goodfellow) as the anode and a platinum (Pt) sheet as the cathode with 2 cm distance. Before anodization, the Ti foil was cleaned in an ultrasonic bath for 30 min in isopropanol followed by 30 min in acetone, rinsed with water and dried in air. The electrochemical anodization was performed in an ethylene glycol electrolyte with 0.25 wt% NH_4F and 2 wt% H_2O. A voltage of 60 V was supplied by a programmable DC power supply (Keithley Instruments model 2200-72-1DC) for 2 h at room temperature. Then, the nanotube film was removed to generate a template for the second step in order to grow highly ordered nanotubes. The second anodization step was carried out by using identical experimental conditions to the first step, but the anodization time was 5 min. To improve the adhesion of the film, the electrodes were left in the anodization solution for 1 h and then well-adhered amorphous TNTs were obtained (Fig. 1) [17].

The as received amorphous TNTs were chemically reduced by CaH_2 to generate highly conducting black TNTs (bTNTs) electrodes (refer to our previous works in [15,16]). Specifically, the TNTs were embeded in 0.2 g of CaH_2 powder in a quartz ampule under vacuum ($<10^{-2}$ Pa) and then annealed at 500 °C for 2 h with heating and cooling rates of 2 °C/min. After annealing, the electrodes were rinsed with deionized water and finally dried in air.

2.2. Enzyme expression, purification and activity essay

The expression of recombinant Fd-HydA1 in *Escherichia coli* was based on the methods described in a previous study [18]. The encoded sequence of hydrogenase was from *Chlamydomonas reinhardtti* HydA1, while the N-terminal tag was from *C. reinhardtii* PetF [2Fe2S]-ferredoxin (Fd). The enzyme expression and purification processes were monitored through measurements of the enzyme concentration both in the lysate and in the elution fractions by running sodium dodecyl sulphate–polyacrylamide gel electrophoresis (SDS-PAGE) and staining with Coomassie blue. The enzyme was enriched in elution fractions compared to lysate. The purified product was verified by Western blot using anti-Strep-tag antibody: a unique band correlated to Fd-HydA1 at 59 kD was detected in cell lysate and enriched in the elution fractions, showing the successive purification of Fd-HydA1, as shown in Fig. 2. Purified Fd-HydA1 had an activity for hydrogen production of 6 μmol/min·mg that was measured by using reduced methyl viologen (MV – 100 mM) as an electron donor.

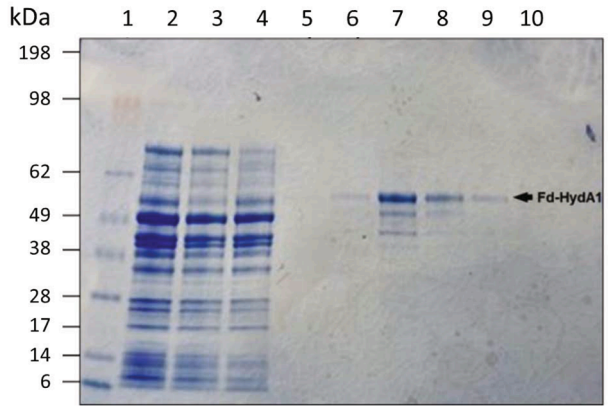

Fig. 2. SDS-PAGE analysis of Fd-HydA1 expression and purification. (*Lane 1*) SeeBlue Plus2 (ThermoFisher Scientific) pre-stained protein standard with molecular size in kDa, (*Lane 2*) lysate fraction, (*Lane 3*) StrepTrap flow-through fraction, (*Lane 4*) first StrepTrap wash fraction, (*Lane 5*) third StrepTrap wash fraction, (*Lane 6-10*) StrepTrap elution fractions.

2.3. Enzyme attachment assays

Nanotube internal walls were exposed by scratching the bTNTs films with a scalpel to crack open the tubes and simultaneously detach them from the Ti foil. The material released was collected in H_2O and ultrasonicated to further separate the nanotubes. The suspension was then drop casted onto a lacey carbon copper grid and dried at room temperature. A drop of freshly purified Fd-HydA1 (10 ng/ml) was deposited on Parafilm® and the copper grids with attached bTNTs were allowed to float for 30 min on the solution drop. The grid was then rinsed with Phosphate-buffered saline (PBS) to remove unbound enzyme molecules and transferred to a drop of blocking solution (2.5% milk, PBS, 0.1% Tween® 20 Detergent) with 1 μL primary antibody (rabbit Anti-Strep-tag II, 1:100, by Abcam, Cat. No: ab76949), incubated for 1 h and subsequently rinsed with PBS. Protein A gold (PAG) solution (University of Utrecht) with particle size of 10 nm was diluted in cold fish gelatin (1:50) and drop casted on Parafilm® where the same grids floated for 1 h before rinsing with H_2O. The samples were then fixated in 2.5% glutaraldehyde phosphate buffer (GPB - Electron Microscopy Science Inc.), rinsed with H_2O and air dried. Negative controls were prepared following the same protocol but excluding the Fd-HydA1 incubation step.

2.4. Vacuum assisted enzyme loading

Dried substrates were immersed into a solution containing Fd-HydA1 (10 ng/ml) diluted in PBS (1:20) under vacuum (CITOVAC, STRUERS) for 15 min to allow infiltration of the nanotubes. Since the enzyme

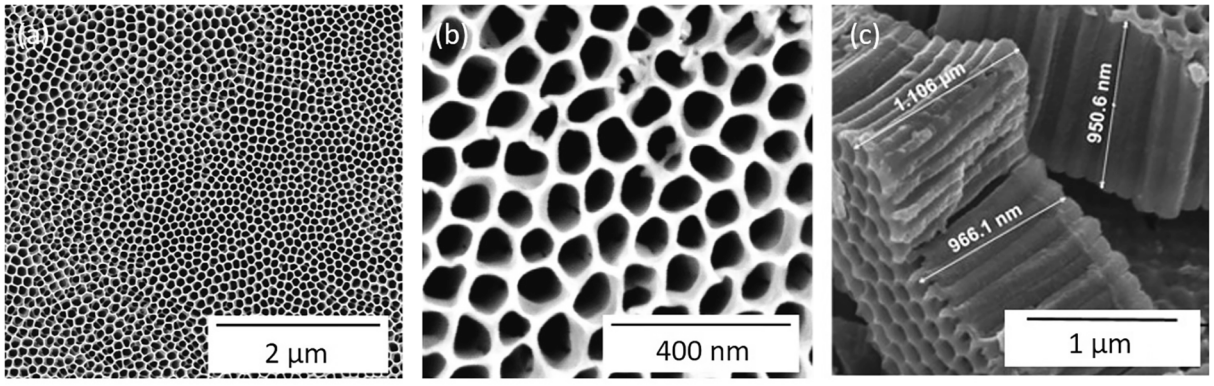

Fig. 1. SEM images of bTNTs. (a) and (b) top view of bTNTs with tube opening size around 140 nm. (c) Side view of bTNTs with nanotube length of around 1 μm.

molecules in the nanotubes could be inaccessible to the subsequently infiltrated immunogold labels, two sample preparation methods were employed:

2.4.1. Immunogold labelling of whole substrates

The enzyme-loaded pieces were incubated in 2 mL 5% blocking solution with 1 μL primary antibody for 1 h at room temperature. After incubation, the enzyme-loaded pieces were washed in PBS and further incubated for 1 h in PAG diluted in cold fish gelatin. The materials were then rinsed in H_2O, fixated with 2.5% GPB, rinsed again and air dried.

2.4.2. Nanotube opening and detachment followed by immunogold labelling

The enzyme-loaded bTNTs films were scratched to crack open the nanotubes and release them from the Ti foil, after which they were collected in PBS. This suspension was drop casted onto lacey carbon copper grids that were transferred to drops of 2.5% blocking solution with antibody, incubated for 1 h and subsequently rinsed with PBS. PAG diluted in cold fish gelatin was drop casted on Parafilm® where the grids were made to float for 1 h before rinsing with PBS. The samples on the grids were fixated in 2.5% GPB rinsed with H_2O and air dried. Negative controls were prepared following the same protocol but excluding the Fd-HydA1 incubation step.

2.5. Magnetically assisted loading

Ferromagnetic nanoparticles (NPs) were used to evaluate the effect of magnetic field application for particles loading. In these assays, bTNTs substrates (attached to Ti foil) were glued onto the flat base of a glass vial with 1 mm of thickness and placed onto a NdFeB magnet cylinder with a diameter of 5 cm, 2 cm of thickness and lifting capacity of 160 kg (SuperMagnet, Norway). Deionized water was infiltrated into the nanotubes with vacuum assistance. The H_2O was then replaced by a suspension of Fe_2O_3 NPs with 25 nm (5 mg/ml, Sigma Aldrich) diluted in PBS (1:2). To mitigate clogging of the nanotubes at the top surface, the magnet with the attached vial were anchored to a shaking tray and the set was gently rocked on and off (30 min/30 min) during an incubation period of 12 h.

2.6. Electron microscopy

The characterization of the bTNTs, as well as the detection of Fd-HydA1 in/on bTNTs, was performed by field-emission scanning electron microscopy (FEG-SEM) using an FEI NOVA NANOSEM 650 in high vacuum settings (10^{-7} Pa) with acceleration voltages in the 5–15 kV range. Scanning transmission electron microscopy (STEM) was performed with a DCOR Cs probe-corrected FEI Titan G2 60-300 instrument with 0.08 nm of nominal spatial resolution. Bright field (BF) and high-angle annular dark field (HAADF) images were acquired simultaneously. Chemical information was obtained by X-ray energy dispersive spectroscopy (EDS) with a Bruker SuperX EDS system, comprising four silicon drift detectors. Several methods were employed for sample preparation:

2.6.1. Detached bTNTs (attachment assays and enzyme loading with vacuum assistance)

The nanotubes dispersed on lacey carbon copper grids were directly characterized by STEM/EDS.

2.6.2. Cross-sections of enzyme-loaded substrates with vacuum assistance

The substrates loaded with enzyme and immunogold labelled were prepared in two ways: (i) surface scratched to expose regions below the surface followed by carbon coating to avoid charging effects during observation; and (ii) embedded in epoxy (Epoxy Embedding Medium kit, Sigma Aldrich) followed by curing at 65° C for 24 h and then cross-sectioned. The cross sections were prepared by standard materialographic techniques involving grinding with SiC paper of decreasing grain size and lapping with a sequence diamond suspension of 6, 3, 1 and ¼ μm each for 5 min at 300 rpm. Both types of cross-sections were characterized by SEM/EDS.

2.6.3. Fe_2O_3-loaded substrates with magnetic assistance

Following nanotube loading with iron oxide, the substrates were air dried. The nanotube film was gently removed from the Ti foil using adhesive tape (TESA 4204). The adhesive tape with attached bTNTs was embedded in epoxy, and the block was sectioned with a cryo-ultramicrotome (Reichert FCS). The sections were deposited on lacey carbon copper grids, dried, carbon coated and finally observed by STEM/EDS.

2.7. Electrochemistry

Electrochemical experiments were carried out in hydrogen-saturated 0.1 M PBS solution with pH 7.2. Cyclic voltammetry (CV) was used to characterize the immobilized Fd-HydA1 on bTNTs as working electrode, with a carbon rod as a counter electrode and saturated calomel electrode (SCE) as the reference. The scan rate was 5 mV/s. The reported potentials were corrected against the reversible hydrogen electrode (RHE) by the equation:

$$E_{RHE} = E_{meas} + pH \times 0.059 + 0.242 \quad (1)$$

where E_{meas} is the measured potential vs SCE and 0.242 is the standard SCE potential vs. the standard hydrogen electrode.

3. Results and discussion

Fig. 3 shows STEM images of Fd-HydA1 attached to bTNTs previously cracked open and released from the Ti foil (enzyme attachment assays). The bright regions in the HAADF image (Fig. 3a) and dark regions in the BF image (Fig. 3b) correspond to gold nanoparticles (Au NPs) and indicate immobilized Fd-HydA1 on the bTNTs walls. Whereas in the control samples, Au NPs could not be detected (Fig. 3c). These results show that Fd-HydA1 can attach to and be immobilized on the surface of bTNTs, further attesting that immunogold labelling can be utilized to visualize immobilized enzyme on support materials.

As mentioned previously, it was important to clarify whether the enzymes entered the high aspect-ratio nanostructures. Immunogold labelling of whole substrates loaded with enzyme showed that most Fd-HydA1 attached on the top surface of the bTNTs film, but very few Au NPs can be found on the interior walls, despite of the vacuum assistance (Fig. 4). Similar results were obtained with immunogold labelling of nanotubes opened and detached after loading. These results suggest impaired diffusion of the enzyme into the nanotubes and clogging effects due to enzyme accumulation on the top region of the tube openings.

In order to explore this hypothesis , we utilized a strong magnetic field to create a direct driving force for suspended Fe_2O_3 NPs (25 nm) to infiltrate the nanotubular structure with 140 nm of average tube opening size. Fig. 5 shows again the absence of any significant amount of Fe_2O_3 NPs inside the nanotubes, reflecting the difficulty to infiltreate the NPs into the nanotubes. In addition to clogging, the present results indicate that the nanofluidic configuration may result from large hydrodynamic radius and steric hindrance from viscous drag near the nanotube walls [19,20]. Occasionally, NPs could be found as deep as 1 μm into the nanotubes, suggesting that a fundamental understanding of the loading process requires theoretical modelling and that the method may be experimentally optimized through geometric modification of the nanotubes and chemical functionalization of their internal walls.

The present immunogold labelling results show that Fd-HydA1 can be successfully attached to immediately available surfaces of the bTNTs support. In addition, the characterization methods described are suitable to attest molecular attachment to internal walls of nanotubes and nanoparticle infiltration of nanostructures. In the case of TNTs, the films

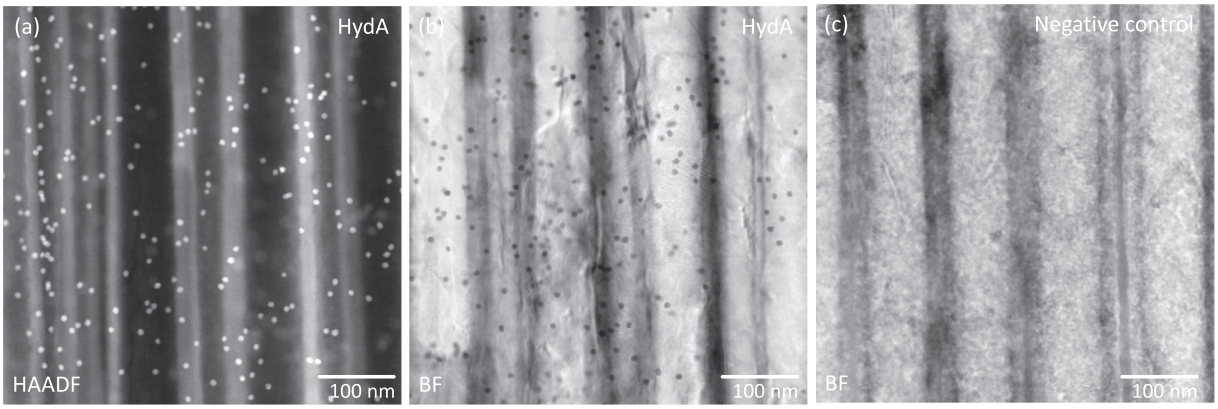

Fig. 3. STEM micrographs obtained from an enzyme attachment assay (see sections 2.3 and 2.6.1). (a) HAADF and (b) BF images of nanotube walls where the high mass Au NPs show the position of attached Fd-HydA1. (c) Negative control.

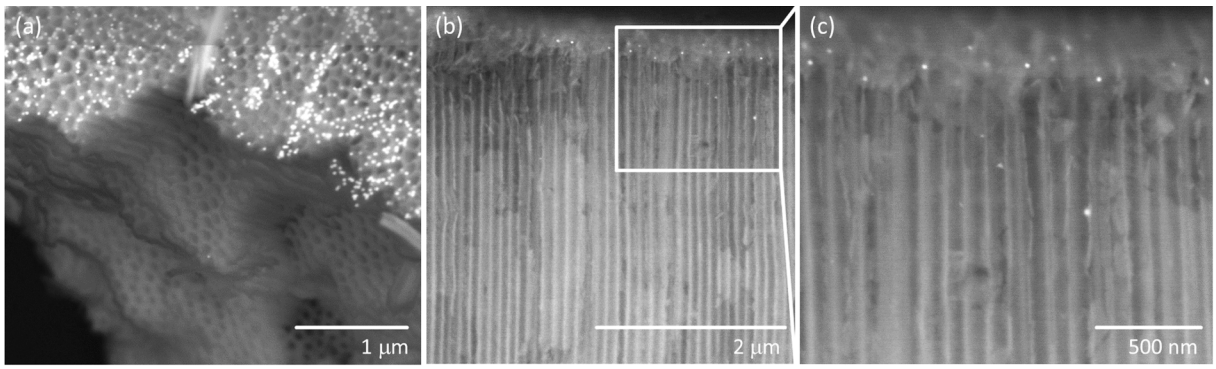

Fig. 4. SEM images in backscattered electron mode after Fd-HydA1 loading with vacuum assistance (described in section 2.4.1) where the bright particles correspond to Au labels. (a) Scratched sample (see section 2.6.2 (i)), (b) and (c) cross-sections (see section 2.6.2 (ii)).

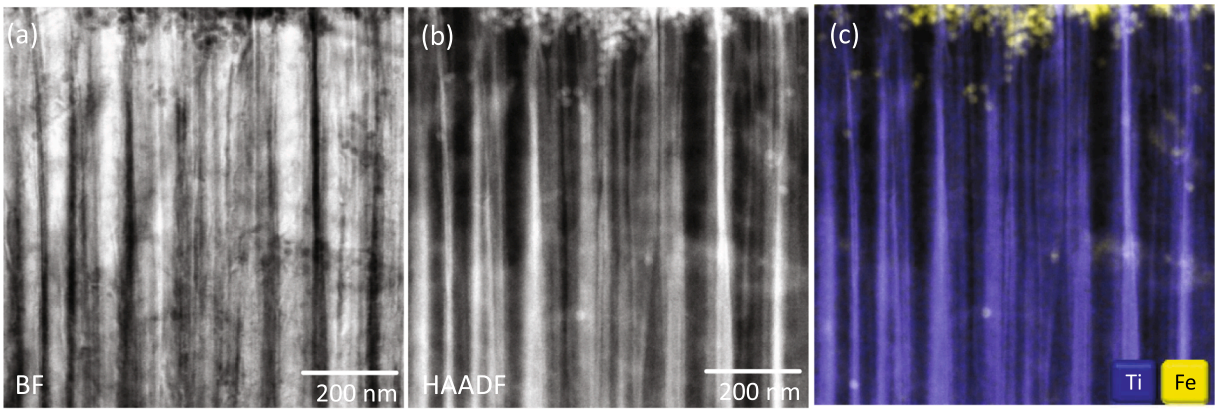

Fig. 5. STEM/EDS results of Fe_2O_3 NPs loaded into bTNTs with magnetic assistance (section 2.5). (a) BF and (b) HAADF images of nanotubes after Fe_2O_3 loading. (c) Corresponding EDS map.

typically present defects at the microscale, such as cracks resulting from stress released during growth, where molecules and nanoparticles tend to flow and accumulate, mimicking nanoscale infiltration. Therefore, only the observation of carefully prepared cross-sections revealing the interior of the nanotubes can prove infiltration and determine its depth.

To explore the electronic interaction between Fd-HydA1 and bTNTs, CV was employed, showing a reductive catalytic current at low potentials (Fig. 6). This current is due to hydrogen production on the hybrid electrode and has an onset at potentials slightly above 0 V vs RHE, in good agreement with the expected HER potential and previously reported data [12,21]. Oxidative catalytic currents are also observed during the anodic potential scan, further confirming the successful Fd-HydA1 immobilization and DET. The current density reaches 17 µA/cm^2 at (−100 mV vs RHE), which is comparable to the report on a *Cr*HydA1-gold electrode (with MV as mediator, 40 µA/cm^2) [22], but lower than that of *Cp*HydA/TiO_2 (~150 µA/cm^2) mainly due to the activity difference of hydrogenases [11]. In the control experiments, where no Fd-HydA1 was immobilized on the bTNTs, no catalytic current was observed, indicating the poor catalytic activity of TiO_2 itself towards the HER. Although we cannot discuss presently any possible "shielding" effects by assuming that the nanotubes may provide a relative anaerobic condition in operation under normal atmospheric

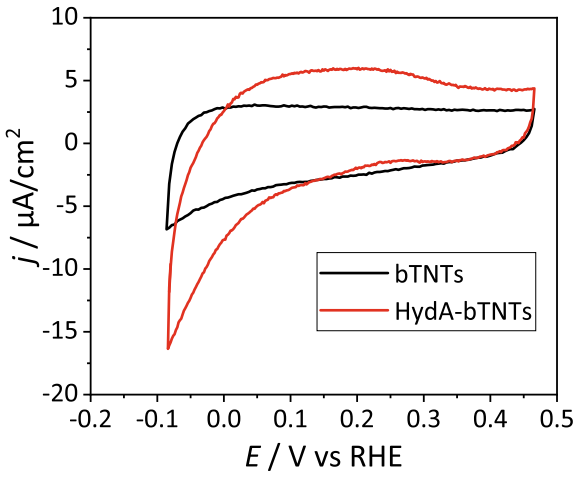

Fig. 6. CV of Fd-HydA1 immobilized on a bTNTs electrode. Controls were performed on bare bTNTs electrodes in PBS solution.

conditions, the interfacial electrochemistry on the Fd-HydA1/bTNTs bioelectrode confirms the DET in the bio-inorganic interface. Even if the Fd-HydA1 molecules would have been successfully inserted in the nanotubes, we may foresee that a clogging of the nanotubes due to gas formation would ultimately decrease the activity of the enzymes. Therefore, further developments and studies on the trade-offs between depth, possible "shielding" and performance are of great importance.

4. Conclusions

By combining STEM and electrochemical measurements, we found that Fd-HydA1 attaches to the outer surface of TNTs, yielding direct electron transfer between black TiO_2 and Fd-HydA1. However, infiltrating the Fd-HydA1 and nanoparticles (gold and Fe_2O_3) into the nanotubes has been proven difficult, suggesting that a stronger driving force and maybe additional activation is required. This may also stem from the strong NPs- or enzyme-TiO_2 interactions, which favor the immobilization/deposition on immediately exposed surfaces and restrict further access into the nanotubes. However, by utilizing the diversity and flexibility of the nanostructured materials, the geometric parameters, such as nanotube opening diameter and length of the nanotubes can be tailored. The systematic optimization of the immobilization and insertion methods, both theoretically and experimentally, are of high demand to enhance the NPs and enzyme immobilization and, furthermore, explore any possible "shielding" effects that high aspect ratio nanostructures can offer to O_2-intolerant enzymes.

CRediT authorship contribution statement

Xin Liu: Investigation, Methodology, Writing – original draft, Writing – review & editing, Validation, Visualization. **Sanne Risbakk:** Investigation, Methodology, Visualization. **Patricia Almeida Carvalho:** Conceptualization, Methodology, Investigation, Visualization, Writing – review & editing, Supervision, Funding acquisition, Project administration. **Mingyi Yang:** Investigation, Visualization, Writing – review & editing. **Paul Hoff Backe:** Methodology, Validation, Resources, Writing – review & editing. **Magnar Bjørås:** Resources, Writing – review & editing. **Truls Norby:** Resources, Writing – review & editing. **Athanasios Chatzitakis:** Conceptualization, Methodology, Validation, Writing – review & editing, Supervision, Funding acquisition.

Declaration of Competing Interest

The authors declare that they have no known competing financial interests or personal relationships that could have appeared to influence the work reported in this paper.

Acknowledgements

This research has been financed by the Research Council of Norway (EnCaSE #275058 and PH2ON #288320).

References

[1] C. Madden, M.D. Vaughn, I. Díez-Pérez, K.A. Brown, P.W. King, D. Gust, A. L. Moore, T.A. Moore, Catalytic turnover of [FeFe]-hydrogenase based on single-molecule imaging, J. Am. Chem. Soc. 134 (2012) 1577–1582.
[2] L. Striepe, T. Baumgartner, Viologens and their application as functional materials, Chem. Eur. J. 23 (2017) 16924–16940.
[3] H. Suo, L. Xu, C. Xu, X. Qiu, H. Chen, H.e. Huang, Y.i. Hu, Graphene oxide nanosheets shielding of lipase immobilized on magnetic composites for the improvement of enzyme stability, ACS Sustain. Chem 7 (2019) 4486–4494.
[4] L. Bayne, R.V. Ulijn, P.J. Halling, Effect of pore size on the performance of immobilised enzymes, Chem. Soc. Rev. 42 (2013) 9000–9010.
[5] C.F. Blanford, F.A. Armstrong, The pyrolytic graphite surface as an enzyme substrate: microscopic and spectroscopic studies, J Solid State Electrochem. 10 (2006) 826–832.
[6] K.A. Vincent, A. Parkin, F.A. Armstrong, Investigating and exploiting the electrocatalytic properties of hydrogenases, Chem. Rev. 107 (2007) 4366–4413.
[7] F. Fernández-Trillo, J.C.M. van Hest, J.C. Thies, T. Michon, R. Weberskirch, N. R. Cameron, Reversible immobilization onto PEG-based emulsion-templated porous polymers by co-assembly of stimuli responsive polymers, Adv Mater 21 (2009) 55–59.
[8] G.L. Drisko, A. Zelcer, V. Luca, R.A. Caruso, G.J.d.A.A. Soler-Illia, One-pot synthesis of hierarchically structured ceramic monoliths with adjustable porosity, Chem Mater 22 (2010) 4379–4385.
[9] H.H.P. Yiu, M.A. Keane, Enzyme–magnetic nanoparticle hybrids: new effective catalysts for the production of high value chemicals, J. Chem. Technol. Biotechnol. 87 (2012) 583–594.
[10] D.H. Nam, J.Z. Zhang, V. Andrei, N. Kornienko, N. Heidary, A. Wagner, K. Nakanishi, K.P. Sokol, B. Slater, I. Zebger, S. Hofmann, J.C. Fontecilla-Camps, C. B. Park, E. Reisner, Solar water splitting with a hydrogenase integrated in photoelectrochemical tandem cells, Angew. Chem. Int. Ed. 57 (2018) 10595–10599.
[11] S. Morra, F. Valetti, V. Sarasso, S. Castrignanò, S.J. Sadeghi, G. Gilardi, Hydrogen production at high Faradaic efficiency by a bio-electrode based on TiO2 adsorption of a new [FeFe]-hydrogenase from Clostridium perfringens, Bioelectrochemistry 106 (2015) 258–262.
[12] S. Morra, F. Valetti, S.J. Sadeghi, P.W. King, T. Meyer, G. Gilardi, Direct electrochemistry of an [FeFe]-hydrogenase on a TiO2 electrode, Chem. Commun. 47 (2011) 10566–10568.
[13] H. Tsuchiya, P. Schmuki, Less known facts and findings about TiO2 nanotubes, Nanoscale 12 (2020) 8119–8132.
[14] Y.-C. Nah, I. Paramasivam, P. Schmuki, Doped TiO2 and TiO2 nanotubes: synthesis and applications, ChemPhysChem 11 (2010) 2698–2713.
[15] A. Touni, X. Liu, X. Kang, P.A. Carvalho, S. Diplas, K.G. Both, S. Sotiropoulos, A. Chatzitakis, Galvanic deposition of Pt nanoparticles on black TiO2 nanotubes for hydrogen evolving cathodes, ChemSusChem 14 (2021) 4993–5003.
[16] X. Liu, P. Carvalho, M.N. Getz, T. Norby, A. Chatzitakis, Black anatase TiO2 nanotubes with Tunable orientation for high performance supercapacitors, J. Phys. Chem. C 123 (2019) 21931–21940.
[17] A. Chatzitakis, M. Grandcolas, K. Xu, S. Mei, J. Yang, I.J.T. Jensen, C. Simon, T. Norby, Assessing the photoelectrochemical properties of C, N, F codoped TiO2 nanotubes of different lengths, Catal. Today 287 (2017) 161–168.
[18] I. Yacoby, L.T. Tegler, S. Pochekailov, S. Zhang, P.W. King, P.D. Riggs, Optimized expression and purification for high-activity preparations of algal [FeFe]-hydrogenase, PLOS ONE 7 (2012) e35886.
[19] L. Bocquet, E. Charlaix, Nanofluidics, from bulk to interfaces, Chem. Soc. Rev. 39 (2010) 1073–1095.
[20] W. Sparreboom, A. van den Berg, J.C.T. Eijkel, Principles and applications of nanofluidic transport, Nat. Nanotechnol 4 (2009) 713–720.
[21] M. Hambourger, M. Gervaldo, D. Svedruzic, P.W. King, D. Gust, M. Ghirardi, A. L. Moore, T.A. Moore, [FeFe]-Hydrogenase-catalyzed H2 production in a photoelectrochemical biofuel cell, J. Am. Chem. Soc. 130 (2008) 2015–2022.
[22] H. Krassen, S. Stripp, G. von Abendroth, K. Ataka, T. Happe, J. Heberle, Immobilization of the [FeFe]-hydrogenase CrHydA1 on a gold electrode: design of a catalytic surface for the production of molecular hydrogen, J. Biotechnol. 142 (2009) 3–9.